

Dusty plasma diagnostics methods for charge, electron temperature, and ion density

Bin Liu,¹ J. Goree,¹ V. E. Fortov,² A. M. Lipaev,² V. I. Molotkov,² O. F. Petrov,² G. E. Morfill,³ H. M. Thomas,³ and A. V. Ivlev³

¹Department of Physics and Astronomy, The University of Iowa, Iowa City, Iowa 52242, USA

²Joint Institute for High Temperatures, Russian Academy of Sciences, Moscow 127412, Russia

³Max-Planck-Institut für extraterrestrische Physik, 85748 Garching, Germany

(Received 15 January 2010; accepted 29 March 2010; published online 7 May 2010)

Diagnostic methods are developed to measure the microparticle charge Q and two plasma parameters, electron temperature T_e , and ion density n_i , in the main plasma region of a dusty plasma. Using video microscopy to track microparticles yields a resonance frequency, which along with a charging model allows an estimation of Q and T_e . Only measurements of microparticle position and velocity are required, unlike other methods that use measurements of T_e and plasma parameters as inputs. The resonance frequency measurement can also be used with an ion drag model to estimate n_i . These methods are demonstrated using a single-layer dusty plasma suspension under microgravity conditions. © 2010 American Institute of Physics. [doi:10.1063/1.3400225]

I. INTRODUCTION

A dusty plasma (also termed complex plasma) consists of microparticles that are suspended in an ionized gas. Dusty plasma is a topic of interest in astrophysics,¹ plasma physics, and industrial processing of semiconductor chips.² It has also attracted great interest in condensed matter physics.^{3–6} A suspension of microparticles exhibits structures and dynamics that are suitable to study some fundamental issues in condensed matter physics.^{7–14} Basic dusty plasma experiments are often performed in glow-discharge plasmas,^{14–22} which have a main plasma region with a small electric field, bounded by sheaths near electrodes where the electric field is much larger, Fig. 1(a). Observations of microparticle motion have been used to diagnose not only parameters such as charge for the dust particles,^{23–25} but also plasma parameters, such as the electric field in a sheath.^{26,27} In the past, many of these efforts have been focused on the sheath region of the plasma, but here we will focus on the main plasma region.

When immersed in a plasma, microparticles are charged. When the charge Q is known, one can estimate the microparticle surface potential ϕ_s as

$$\phi_s = Q/4\pi\epsilon_0 a, \quad (1)$$

where a is the microparticle radius.²⁸

Microparticles are electrically confined either in a main plasma or a sheath. In a ground-based experiment, micron-size microparticles settle in the sheath, where the electric force $F_E = QE_{dc}$ can balance the force due to gravity $m_p g$. Here m_p is microparticle mass and E_{dc} is the dc electric field. Under microgravity, microparticles are positioned not in the high E_{dc} field region of a sheath, but in the weak E_{dc} field region of the main plasma. In the absence of gravity, the force due to flowing ions becomes important. This ion drag force, F_{ID} , opposes the inward force due to E_{dc} , leaving a void near the plasma center.^{21,29,30} Here, we will develop analysis methods useful in the main plasma region, and we

will demonstrate them using an experiment performed under microgravity conditions, with a void.

One approach to determine the charge Q of a microparticle immersed in a plasma is to use a theoretical charging model. Such models require, as their inputs, values for plasma parameters such as electron temperature T_e , ion flow velocity v_i , and sometimes plasma density n_i . However, precise measurements of these input parameters are generally more difficult than measurements of microparticle positions and velocities, and some microgravity plasma instruments are not equipped to measure these parameters. Therefore, to measure Q , we will develop here a method that makes use of measurements of microparticle positions but not of T_e . Previous methods of measuring Q are reviewed in Appendix A. Our approach is different because it makes use of a charging model in combination with simple models for a gas-discharge plasma, so that the required inputs are only microparticle position and velocity, gas pressure, and gas temperature. These inputs can be measured with more accuracy than most plasma parameters.

Here we will develop a different resonance method of measuring charge. This method also involves a measurement of resonance frequency ω_R and an assumption for E_{dc} . However, our resonance method is different from the method of Melzer and co-workers^{31,32} in several ways: It is intended for use in the main plasma, it requires models for charging and a relationship between E_{dc} and T_e , and it does not require a measurement of T_e and n_i .

Along with our resonance method, we also develop here a force-balance method to measure n_i . Our two diagnostics methods are intended for measuring dusty plasma parameters in the main plasma region. They can be used separately or together. When used together, they yield Q for the microparticles, two plasma parameters, T_e and n_i . Both methods are applicable to dusty plasma experiments with a few layers of microparticle suspension in a steady state, where micro-

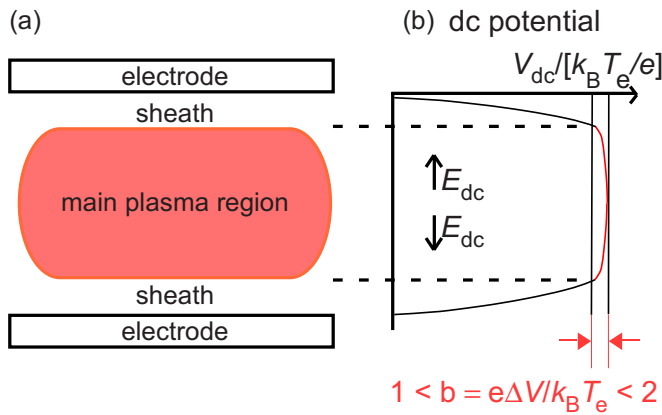


FIG. 1. (Color online) Sketch of a glow-discharge plasma. (a) The main plasma region is bounded by sheaths, which have a deficit of electrons and a strong electric field. (b) The time-averaged (dc) electric potential has positive peak. In the main plasma, from the sheath edge to the center, the height of this peak is a multiple of one or two times $k_B T_e / e$. The dc electric field E_{dc} points away from the main plasma, expelling ions.

particles undergo mostly random motion and their positions can be measured accurately.

In this paper, we will introduce these two methods and demonstrate them using an experiment. In Sec. II we will present these two methods in detail. In Sec. III, we will present the demonstration experiment of our methods of measuring Q , T_e , and n_i .

II. METHODS

A. Resonance method to determine Q and T_e

The resonance method is based on a measurement of the resonance frequency ω_R of microparticles. We will describe how it is used for microparticles that are located in a thin layer near the edge of a void. The resonance method yields values for Q and T_e , in five steps as detailed below.

The first step yields a value for the force constant k . We start with a measurement of resonance frequency, ω_R . The resonance frequency can be measured either by tracking random motions of unmanipulated microparticles, as in Ref. 21, or by some manipulation scheme.^{31–33} This resonance frequency is combined with the known mass of microparticles to yield the force constant k . This step requires no major assumptions other than linear harmonic motion, and it has no free parameters.

The second step yields values for the dc electric force F_E , calculated using the force constant k from the first step. For the main plasma region of interest here, we will calculate this as

$$F_E = -ckz, \quad (2)$$

where the factor c accounts for the contribution of the electric force to k , and z is the equilibrium height of microparticles, which is measured from the plasma center to the microparticles.

To calculate F_E using Eq. (2) requires an estimation of the value for c . Here, instead of estimating a single value for c , we will perform all our calculations using several values in

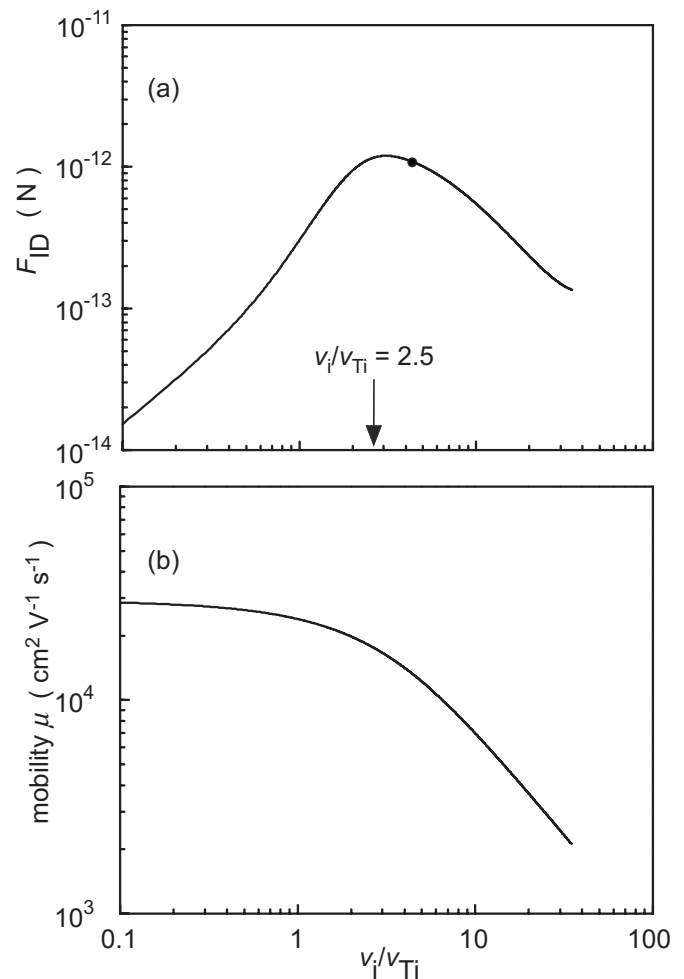


FIG. 2. (a) Dependence of ion drag force F_{ID} on ion flow velocity v_i . Due to acceleration by E_{dc} , v_i generally increases with distance from the plasma center. An equilibrium occurs when $F_{ID} + QE_{dc} = 0$, as indicated for example by the dot. This depends on parameters such as ion density and microparticle charge, which may vary with position. (b) Dependence of ion mobility coefficient μ on v_i . Data shown here are calculated for typical experimental parameters: microparticle radius $a = 3.4 \mu\text{m}$, a 0.12 torr neon gas, and plasma parameters $T_e = 2.3 \text{ eV}$, $T_i = 0.025 \text{ eV}$, and $n_i = 2.3 \times 10^8 \text{ cm}^{-3}$.

a range. Later, when used with our force-balance method and an iterative process, we can obtain a single value for c .

To estimate a range for c , we discuss here the contributions to k due to F_E and F_{ID} . Since the force constant k arises from the spatial derivative of the net force $\mathbf{F}_{ID} + \mathbf{F}_E$, the spatial scalings of these two forces determine the value for c . The electric force F_E is generally proportional to E_{dc} (which varies with position in a glow-discharge plasma), so F_E always contributes to k . The contribution due to F_{ID} , however, varies greatly with ion flow velocity

$$v_i = \mu E_{dc}, \quad (3)$$

where μ is mobility, because both F_{ID} and μ vary with v_i , as shown in Fig. 2, for typical experimental parameters. We will consider, as examples, two cases for F_{ID} . For the case where $v_i / v_{Ti} \approx 2.5$ (here v_{Ti} is ion thermal velocity), F_{ID} has its peak value and varies little with v_i , so the contribution of F_{ID} is weak, and k arises almost entirely due to F_E ,²¹ i.e., $c = 1$. For the case where $v_i / v_{Ti} \gg 2.5$ and $F_{ID} \propto v_i^{-2}$, both F_E and

F_{ID} contribute to k , it can be shown that $c \geq 0.3$ (Appendix B). These values can be used to guide us in choosing initial guesses for the value of c , in our iteration process described later.

The third step yields a curve on a graph of Q versus T_e . We will use

$$Q = F_E/E_{dc} \quad (4)$$

with F_E from the second step. We will consider the dc electric field E_{dc} has two contributions, $E_{dc} = E_{dc,ei} + E_{dc,p}$, where $E_{dc,ei}$ is due to the ambipolar transport of electrons and ions, and $E_{dc,p}$ is due to microparticles. In many dusty plasmas, the interparticle force $QE_{dc,p}$ is important, but here we will consider cases where there are few microparticles, for example only a single layer of microparticles at a void edge. In this case of few microparticles, we will approximate that $E_{dc,p}$ is negligible and $E_{dc} \approx E_{dc,ei}$. This will allow us to estimate E_{dc} using a simple model for a dust-free gas-discharge plasma. Here we assume small-amplitude motion, so that we can neglect the variation in Q with position during the oscillatory movement of a microparticle. In our simple model of E_{dc} , we will use $E_{dc,ei} = -\nabla V_{dc}$, the Boltzmann response for electron density, $n_e \propto \exp(eV_{dc}/k_B T_e)$, and assume that the plasma has a uniform T_e and an electron density that varies with position. Combining these assumptions yields $E_{dc,ei} = -k_B T_e \nabla n_e / en_e$. Thus, $E_{dc,ei}$ is proportional to T_e and inversely proportional to a plasma scale length L . We express this scaling as

$$E_{dc,ei} = bk_B T_e / eL. \quad (5)$$

Here, b is an unknown parameter that quantifies the potential drop ΔV across the main plasma region, as sketched in Fig. 1(b). For low-power symmetrically driven rf plasmas of the type used in microgravity dusty plasma experiments, b typically varies from 1 to 2.^{34–36} While the parameter b is constrained to a narrow range, it is not a constant: It can vary with position and it can vary from one plasma to another. Using Eq. (5) in Eq. (4) yields a curve in a graph of Q versus the free parameter T_e .

The fourth step yields another curve for Q versus T_e . This is done using data for ion mobility μ (based on gas pressure measurements and Eq. (14) of Ref. 37). In our fourth step, we combine Eq. (3) with two models: E_{dc} as a function of T_e using Eq. (5), and a charging model that has T_e and v_i as its inputs. For E_{dc} , here we will use $E_{dc,ei}$ from Eq. (5), which is suitable for cases where there are few microparticles (although in general one could use some other input for E_{dc} that takes into account interparticle interactions). One could choose among various charging models. One popular model is the orbital-motion-limited (OML) ion-current model, which requires $a \ll \lambda_D \ll \lambda_i$, where a is microparticle radius, λ_D is the Debye length, and λ_i is ion mean-free path. For the demonstration experiment presented in Sec. III, we will use the OML model²⁸ for ion current. Using inputs for T_e and v_i , the OML model yields a value for Q based on the balance of electron and ion fluxes to a single microparticle,³⁸ which can be found from the root ξ of the current balance equation

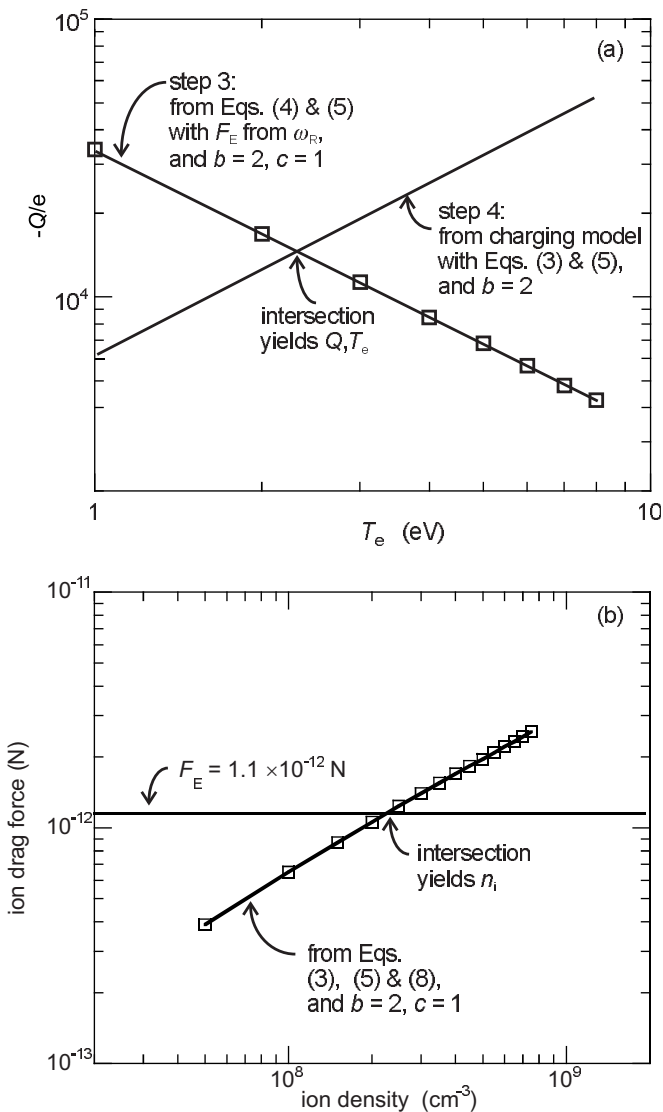


FIG. 3. (a) Demonstration of the final step of our resonance method of estimating Q and T_e simultaneously. The downward and upward-sloping curves are the solutions from steps 3 and 4, respectively, as functions of the unknown parameter T_e . Their intersection yields for the values of both Q and T_e . (b) Demonstration of our force-balance method of estimating n_i . The horizontal line represents a constant value for F_E , while the upward-sloping line represents ion drag force variation with ion density. The intersection yields the result for the value of ion density.

$$2v_{Te} \exp(\xi) - v_{Ti} u^{-1} \times \left[\sqrt{\frac{\pi}{2}} (1 + u^2 + 2\xi\tau) \operatorname{erf}\left(\frac{u}{\sqrt{2}}\right) + u \exp\left(-\frac{u^2}{2}\right) \right] = 0. \quad (6)$$

Here, v_{Te} is the electron thermal velocity, $\xi = |Q|e/aT_e$, $u = v_i/v_{Ti}$, $\tau = T_e/T_i$, and T_i is the ion temperature, which is often comparable to the gas temperature in low-power weakly ionized plasmas.

In our fifth step, we find the intersection of the two curves for Q versus T_e that were found in the third and fourth steps. This is illustrated in Fig. 3(a). This intersection yields our result for the resonance method, a value for Q and T_e .

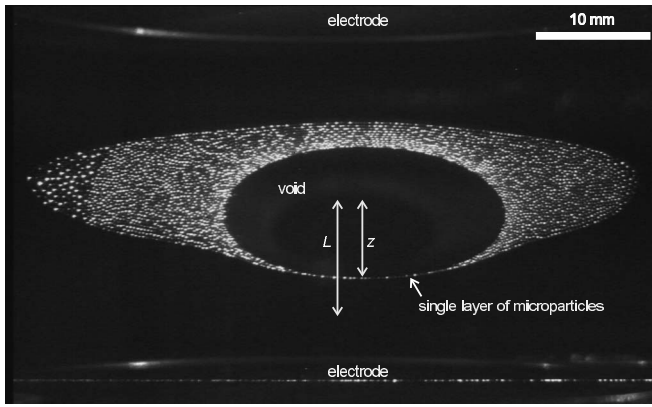


FIG. 4. Side-view image of the microparticle suspension in our demonstration experiment. In this still image from a video recording, microparticles appear as white spots, due to illumination by a vertical sheet of laser light. An analysis of the video yields the small-amplitude motion and equilibrium positions of microparticles in the single layer (at the bottom of the void), which are used as the inputs for our two methods. Distances are measured from the plasma center, half-way between the electrodes.

The accuracy of this resonance method is mainly determined by the models that are used for charging and for dc electric field in a gas-discharge plasma. The results for Q and T_e are also sensitive (but not strongly sensitive) to the choices for c and b , as we will determine in Sec. III. Among the various inputs for this model, one of the most accurate is the resonance frequency measurement.

B. Force-balance method to determine n_i

The ion density n_i is determined by force balance on a single microparticle

$$\mathbf{F}_E + \mathbf{F}_{ID} = 0, \quad (7)$$

where we have assumed that the force balance is determined only by the electric force F_E and the ion drag force F_{ID} , neglecting the gravity and thermophoresis. The force-balance method could be used for experiments under microgravity conditions, or in laboratory experiments where thermophoresis cancels gravity.³⁹

The force balance in Eq. (7) will yield a value for n_i because F_{ID} is proportional to n_i . One way of presenting the balance in Eq. (7) is graphically, as illustrated in Fig. 3(b). Using a model for F_{ID} , one computes the upward-sloping curve in Fig. 3(b). Its intersection with the constant value of F_E yields the result for this method, a value for n_i .

The force-balance method requires an input for F_E . There are several ways to obtain a value for F_E . In our demonstration experiment, in Sec. III, we will use an estimate of F_E generated by our resonance method, Sec. II A, although one could instead use some other method, for example calculating F_E using Eq. (4) with values of Q and E_{dc} obtained from some other experimental method or simulation.

Our force-balance method also requires a theoretical model to calculate F_{ID} . While our method could be used with any suitable ion drag model, for the purpose of demonstrating our method in Sec. III, we will use the Khrapak ion drag model.³⁸ This model assumes $a \ll \lambda_D \ll \lambda_i$. The key prediction of this model, Eq. (18) of Ref. 38, is

$$F_{ID} = \sqrt{2\pi} a^2 n_i m v_{Ti}^2 \left\{ \sqrt{\frac{\pi}{2}} \operatorname{erf}\left(\frac{u}{\sqrt{2}}\right) \times [1 + u^2 + (1 - u^{-2})(1 + 2\xi\tau) + 4\xi^2 \tau^2 u^{-2} \ln \Lambda] + u^{-1}(1 + 2\xi\tau + u^2 - 4\xi^2 \tau^2 \ln \Lambda) \exp\left(-\frac{u^2}{2}\right) \right\}, \quad (8)$$

where m is ion mass, $\ln \Lambda = \ln[(\bar{\beta} + 1)/(\bar{\beta} + a/\lambda_D)]$, $\bar{\beta} = \xi\tau a / [\lambda_D(1 + u^2)]$. Required inputs for this calculation are Q and T_e . In general these inputs could be obtained from any suitable experimental or simulation method; in our demonstration in Sec. III we will use values of Q and T_e from our resonance method, and a value of v_i calculated using Eq. (3).

C. Iteration to eliminate free parameters

When used together, the resonance and force-balance methods yield values for Q , T_e , and n_i , but they require as inputs free parameters b and c . It is desirable to eliminate these free parameters, which we can accomplish by using an iterative process, described here.

We begin by guessing values for b and c , which we will designate b_{in} and c_{in} . We then apply both the resonance and force-balance methods, yielding an estimate of Q , T_e , and n_i , which can then be used to calculate values of the forces F_E and F_{ID} , and a new value for the electric field E_{dc} at the position of the microparticle. Next, we calculate the net force $\mathbf{F}_E + \mathbf{F}_{ID}$ and its spatial derivative, yielding a value for c , which we designate as c_{out} . The ratio of the new and previous values of E_{dc} is b_{out} . Thus, in this first iteration, we start with values b_{in} and c_{in} , and it yields values b_{out} and c_{out} . We can then repeat the iteration, using the previous values of b_{out} and c_{out} as the new b_{in} and c_{in} . This iteration is repeated until the values converge. In a test, we found that convergence to the third digit is achieved after about three or four iterations.

III. DEMONSTRATION EXPERIMENT

We demonstrate our resonance and force-balance methods using data from the experiment in Ref. 21. The experiment was performed under microgravity conditions using the PK-3 Plus instrument on the International Space Station.³⁰ A plasma was generated between a pair of parallel-plate electrodes, which are powered by radio-frequency voltage. Neon gas was introduced at 0.12 torr, and at this pressure, ion motion is expected to be mobility limited. The main plasma region had a thickness $2L = 20$ mm, Fig. 4. The gas temperature was about 300 K.

Melamine-formaldehyde microparticles were injected into the plasma, where they became electrically charged and confined in a suspension. The microparticle radius was $a = 3.4 \mu\text{m}$ with a mass $m_p = 2.5 \times 10^{-13}$ kg; these values are used as inputs for both of our methods. A vertical cross section of the suspension was imaged, revealing that the suspension had a void near the plasma center and a single layer on the lower boundary of the void, Fig. 4.

There was a finite thermophoretic force due to a small temperature gradient of about 0.05 K/cm. This thermophoretic force displaced the suspension upward slightly, so

TABLE I. Results for Q and T_e (from the resonance method), and n_i (from the force-balance method, using Q and T_e as inputs). Results for ϕ_s are computed using Eq. (1). Data shown are from our demonstration experiment. There are two unknown parameters for the resonance method: b relates E_{dc} and T_e in a gas discharge and c quantifies the fractional contribution of F_E to the force constant k , where the remaining contribution arises from F_{ID} . For the force-balance method, b is an unknown parameter. These results demonstrate the methods and their sensitivity to the unknown parameters. An iteration process is also demonstrated to determine the unknown parameters b and c . The final results appear in the last line of this table.

Iteration	Parameters				Results			
	Input		Output		Q ($-e$)	ϕ_s (V)	T_e (eV)	n_i (cm^{-3})
	b_{in}	c_{in}	b_{out}	c_{out}				
0	Initial	Estimates						
	0.5	1	0.65	3.64	2.6×10^4	-11.0	5.2	1.2×10^8
	1	1	1.13	1.74	2.0×10^4	-8.4	3.5	1.4×10^8
	2	1	2.2	1.04	1.5×10^4	-6.3	2.3	2.3×10^8
	0.5	0.5	1.40	1.07	1.9×10^4	-8.0	3.6	2×10^8
	2	0.5	2.35	3.5	1.0×10^4	-4.2	1.6	2.1×10^8
1	2.2	1.04	2.18	1.08				
2	2.18	1.08	2.17	1.06				
3	2.17	1.06	2.17	1.07	1.45×10^4	-6.1	2.27	2.28×10^8

that there was only single layer at the bottom of the void. A single layer such as this is suitable for our resonance method for two reasons: first, it is reasonable to ignore the interparticle interactions $E_{dc,p}$ as well as any electron depletion on the microparticles, and second the equilibrium positions of the microparticles are located a finite distance z from the plasma center. Our force-balance method ignores the thermophoretic force, which is allowable for this experiment, where F_E and F_{ID} were at least 40 times larger than the thermophoretic force.

Using image analysis techniques⁴⁰ that have very small errors, we calculate a microparticle's position with subpixel accuracy. We then track the microparticle by identifying it in the next video frame, and calculating its velocity. From microparticle velocity time series data, we calculate the spectrum for microparticle oscillations in the single layer. Fitting the spectrum to a model for a simple harmonic oscillator, driven by white noise and damped by gas friction, yields the resonance frequency $\omega_R = 25 \text{ s}^{-1}$. Further details of this calculation of ω_R were reported in Ref. 21.

We must assess the validity of the charging model we use in the resonance method and the ion drag model that we use in the force-balance method. This experiment easily satisfies the $a \ll \lambda_D$ requirement of the OML model, but not the low collisionality requirement that the ion-neutral mean-free path should be larger than λ_D . In our experiment, the mean-free path was 1 mm. There were no measurements of λ_D , but a reasonable estimate would be in the range 0.5–2 mm. We use the Khrapak ion drag model,³⁸ which has the same two requirements as for OML. Thus, if the OML and Khrapak ion drag models used here are limited in their validity, it would mainly be due to the ion-neutral collisionality requirement. We will estimate this error in Sec. III A.

A. Demonstration of resonance method for T_e and Q

Results for the first two steps of the resonance method, the force constant k and the electric force F_E , were presented in Ref. 21. As our first step in Ref. 21, using the measured spectrum of random motion, we found $\omega_R = 25 \text{ s}^{-1}$; combining this with the microparticle mass $m_p = 2.5 \times 10^{-13} \text{ kg}$ yielded $k = 2 \times 10^{-10} \text{ N m}^{-1}$. Using this value for k with the observed particle temperature, we calculate the rms displacement of microparticle as $\delta z = 0.005 \text{ mm}$. This displacement is very small, $\delta z/z < 5 \times 10^{-4}$, which justifies our assumption of small-amplitude motion.

In the second step, this value for k is combined with a measured value for $z = 7 \text{ mm}$ to obtain a value for F_E . This result was reported in two cases, $F_E = 5 \times 10^{-13}$ and $1 \times 10^{-12} \text{ N}$, corresponding to $c = 0.5$ and $c = 1$, respectively. These results for the first and second steps were reported in Ref. 21; they are the basis for the remaining steps of our new method of finding Q and T_e , which we present these steps next.

The third and fourth steps of the resonance method yield a pair of curves for Q versus T_e , as illustrated in Fig. 3(a). Here, we only show data for one set of parameters, $b = 2$ and $c = 1$. When a range of values for b and c are used, instead of a single pair of curves, we would have multiple curves. Consequently, in the final step, we will obtain ranges of values instead of a single value, for the results Q and T_e .

In our fifth step of the resonance method, we obtain the values of Q and T_e as the intersection of upward and downward-sloping curves as demonstrated in Fig. 3(a). Because of our multiple values for the unknown parameters b and c , we obtain five intersections, yielding five values for Q and for T_e . We report the values for these five intersections in Table I. These results fell in the range, from -1×10^4 to

-2.6×10^4 for Q/e , and 1.6–5.2 eV for T_e . The corresponding surface potential ϕ_s , computed using Eq. (1), fell in the range $-11.0 < \phi_s < -4.2$ V. The midpoints of these ranges are $Q/e = -18\,000$, $T_e = 3.4$ eV, and $\phi_s = -7.6$ V.

We can compare our result for microparticle charge to previous measurements in microgravity experiments.^{29,41} To allow a comparison of results for different microparticle sizes, we will compare the surface potential ϕ_s . First, we compare to the experiment of Schwabe *et al.*,⁴¹ who used the same PK-3 Plus instrument and the same gas (neon) as us, but a larger 4.6 μm microparticle radius and a slightly higher rf voltage. They made their measurements in a thicker suspension, where electron depletion could be more significant than in our single-layer suspension. Using measurements of density waves propagating away from the void, they found $Q/e = -6200$, corresponding to $\phi_s = -1.9$ V. This floating potential is about a factor of four smaller than our midpoint value of -7.6 V. Second, we compare to the parabolic-flight experiment of Wolter *et al.*,²⁹ who used a different parallel-plate plasma chamber, a different gas, argon, and a thicker suspension, but the same microparticle size as in our experiment. Using a force-balance method, with Langmuir-probe measurements of E_{dc} and n_i as inputs, they found $Q/e = -17\,300$, corresponding to $\phi_s = -7.3$ V. This floating potential is about the same as our result. There is no reason to expect an exact match in comparing our results to these other experiments, since ϕ_s is expected to vary from one experiment to another due to a different value of T_e (which depends on rf voltage, gas type and pressure, and electrode configuration) and different degree of electron depletion (which depends on thickness of the suspension, microparticle size, and microparticle spacing).

As we discussed in Sec. II A, the accuracy of this resonance method is determined by the charging and electric-field models, and the unknown parameters b and c . We have estimated these errors, as we describe next.

As a test to assess the error that might be introduced due to ion-neutral collisionality in the charging model, we repeated our calculations of Q and T_e using Khrapak's collisionality correction to the OML model.⁴² We found that our resonance method yielded a value of T_e that was larger, and Q that was less negative, both by a factor of two, as compared to our results using the OML model.

To assess the sensitivity of Q and T_e to the two unknown input parameters c and b , we use results in Table I. We find the sensitivity of Q to b , $|(\delta Q/Q)/(\delta b/b)|$, ranges from 0.4 to 0.5. Its sensitivity to c , $|(\delta Q/Q)/(\delta c/c)|$, ranges from 0.5 to 0.6. Similarly, the sensitivity of T_e to b is 0.6, and its sensitivity to c is 0.54. Because these sensitivities are all smaller than unity, we note that the accuracy of the resonance method is not greatly diminished by the use of the unknown parameters b and c . As mentioned above, the choice of the charging model can affect the results for Q and T_e by a factor of two. Thus, the accuracy of our resonance method is limited more by the choice of the charging model than by the values of b and c .

B. Demonstration of force-balance method for n_i

The force-balance method centers on Eq. (7), used graphically as illustrated in Fig. 3(b). It yields a value for the ion density n_i , from the intersection of the curves in this graph.

To demonstrate the force-balance method, we again use data from the experiment of Ref. 21. This method requires an ion drag model, and here we will use Khrapak's ion drag model, Eq. (8). It also requires as an input a value for F_E , and here we use values generated by Eq. (2) in our resonance method. As before, we will consider two cases for F_E , corresponding to $c=0.5$ and $c=1$, and three values for the unknown parameter b for the dc electric field E_{dc} . Our results are presented in Table I. We find that the values for n_i fell in the range $(1.2\text{--}2.3) \times 10^8 \text{ cm}^{-3}$.

Our result for n_i is not strongly sensitive to the unknown parameter b . Using the data in Table I for our demonstration experiment, we find that the sensitivity of n_i to b , $|(\delta n_i/n_i)/(\delta b/b)|$, ranges from 0.2 to 0.7. Some of this sensitivity arises from our use, as inputs to the force-balance method, of values for Q and T_e , since these values are sensitive to b . These inputs from the resonance method also lead to a sensitivity of n_i to c ; this sensitivity ranges from 0 to 0.8. Since all these sensitivities are less than unity, we note that the accuracy of the force-balance method is not greatly diminished by the use of the unknown parameters b and c . If the input values for Q and T_e were obtained from some method other than our resonance method, the accuracy of the force-balance method might be further improved.

C. Demonstration of iteration process

Using the resonance and force-balance methods together, our iteration process yields single values for Q , T_e , and n_i , as well as the values for b and c . For the same experiment described earlier, and initially guessing input parameters $b_{\text{in}}=2$ and $c_{\text{in}}=1$, applying our resonance method once yields $Q = -1.5 \times 10^4 e$ and $T_e = 2.3$ eV, and our force-balance method yields $n_i = 2.3 \times 10^8 \text{ cm}^{-3}$. We then improve these estimates using the iteration process as described in Sec. II C. This yields in the last line of Table I our final results $Q = -1.45 \times 10^4 e$, $T_e = 2.27$ eV, and $n_i = 2.28 \times 10^8 \text{ cm}^{-3}$, as well as the parameters $b_{\text{out}} = 2.17$ and $c_{\text{out}} = 1.07$. The accuracy of these results is limited mainly by the accuracy of the charging and ion drag models. The accuracy is no longer limited by estimated values of b and c , since these are improved in the iterative process.

IV. CONCLUSION

While there have been many methods reported for estimating microparticle charge and plasma parameters based on observations of microparticles, many of these methods were developed for microparticles levitated in a sheath. Here we have developed two methods, which can be used separately or together, for microparticles in the main plasma region. Our methods yield results not only for microparticle charge Q , but also for the plasma parameters T_e and n_i .

Our resonance method yields estimates of Q and T_e based on measurements of a resonance frequency for microparticles in the main plasma region. Our force-balance method provides an estimate of n_i using a measurement of electric force.

These methods require only video microscopy measurements of microparticles, and do not require any other diagnostics of plasma parameters. Many space-based microgravity instruments, for example, provide video microscopy but lack diagnostics of plasma parameters; therefore, our methods are well suited for those applications. Our methods may also be useful for ground-based experiments where a thermophoretic force is purposefully introduced to cancel the effects of gravity.

We demonstrated our methods using an experiment under microgravity conditions with single microparticle layer at the void edge. For microparticles of radius $3.4 \mu\text{m}$, our iteration process yielded the charge $Q = -1.45 \times 10^4 e$, the electron temperature $T_e = 2.27 \text{ eV}$, and ion density $n_i = 2.28 \times 10^8 \text{ cm}^{-3}$, for our low-power rf neon plasma. The accuracy of these results is limited primarily by the charging and ion drag models used. The experimental observations that are required (microparticle position, resonance frequency, gas pressure, and temperature) can be measured with considerable precision and do not significantly limit the model's accuracy.

ACKNOWLEDGMENTS

Work at The University of Iowa was supported by NASA Grant No. NNX07AD22G and the NSF Grant 0903501. Work in Russia was supported by RFBR Grant No. 08-02-00444. Gefördert von der Raumfahrt-Agentur des Deutschen Zentrums für Luft und Raumfahrt e. V. mit Mitteln des Bundesministeriums für Wirtschaft und Technologie aufgrund eines Beschlusses des Deutschen Bundestages unter dem Förderkennzeichen 50 WP 0203.

APPENDIX A: REVIEW OF METHODS OF MEASURING MICROPARTICLE CHARGE

Previous methods making use of microparticle observations, together with various assumptions, models, and parameter inputs, are reviewed here. Broadly, we can classify these methods according to whether the microparticle measurement centers on dynamical motion or the equilibrium position under a force balance.

Methods relying on microparticle motion include those using vertical resonance oscillation,^{31,32} the breathing mode,⁴³ and wave dispersion.^{16,41,42,44,45} These all require data from tracking microparticle motion. The vertical resonance method relies on observing a resonance frequency ω_R for microparticles oscillating in a confining electric field; it has so far been applied only to microparticles in an electrode sheath. The resonance method requires a model for electric field. Wave methods require a theoretical model for the frequencies of the wave modes, and this model must assume a particular interparticle interaction. A binary Yukawa potential is usually assumed, ignoring any three-body interactions.

Methods relying on microparticle equilibrium position include those using force balance due to confinement forces, either alone or in combination with mutual interactions. Methods using only confinement forces include calculations using $m_p \mathbf{g} + \mathbf{F}_E = 0$ in a sheath,²⁶ and $\mathbf{F}_{\text{ID}} + \mathbf{F}_E = 0$ near void boundary in main plasma.²⁹ A variation in these methods of analysis has been used with microparticles that are moving at a constant drift velocity,^{42,44} rather than in stationary equilibrium positions. Some of these force-balance methods require theoretical models for ion drag or gas drag forces. Methods using mutual interaction of microparticles require a model for the interaction, such as the binary Yukawa potential; they have been used in several geometries of microparticle confinement.^{24,25,46}

Here, we briefly review the vertical resonance method originally developed by Melzer and co-workers^{31,32} because the method we develop here also makes use of a resonance frequency ω_R . Melzer's resonance method is intended for microparticles levitated in the lower sheath above a horizontal electrode, not in the main plasma region. The charge Q is calculated from a measurement of ω_R , a measurement of n_i in the main plasma, and a free parameter to estimate electron density inside the sheath. It is assumed that microparticles are levitated by a combination of a downward $m_p g$ and an upward F_E in the sheath. A model of the spatial variation in the dc electric field E_{dc} in the sheath is required, and in Melzer's method it is assumed to be linear with height, so that the potential is harmonic. It is also assumed that Q remains constant, neglecting the spatial variation in parameters such as v_i that can affect Q , as microparticles oscillate in positions. (One can generalize this method, by assuming nonharmonic potential²⁷ or nonconstant charge.⁴⁷) Ion drag and thermophoretic forces are assumed to be negligible.

APPENDIX B: ESTIMATION OF PARAMETER c

In Sec. II A, we introduced a parameter c to quantify fractional contribution to the spring constant k due to F_E . Here, we present theoretical estimates of the value of c in the presence of an ion flow typical of experiments.

We show that $c \geq 0.3$ for the case $v_i/v_{Ti} \geq 2.5$. In this high ion-velocity case, the ion drag force is $F_{\text{ID}} \propto v_i^{-2}$,⁴⁸ as can be seen in Fig. 2(a). Also for this velocity range, μ varies with v_i from $\mu \approx \text{const}$ at low v_i to $\mu \propto E^{-1/2}$ at higher v_i ,³⁷ as can be seen in Fig. 2(b). Neglecting the variation in Q with v_i , we have

$$F_E = \alpha E, \quad (\text{B1})$$

$$F_{\text{ID}} = \beta E^{-\zeta}.$$

Here, the exponent ζ is in the range $1 \leq \zeta \leq 2$. The electric field E can be expressed as $E = E_{\text{eq}} + \gamma \delta z$, where δz is the displacement of microparticle. Using the force balance at equilibrium, $\alpha E_{\text{eq}} = \beta E_{\text{eq}}^{-\zeta}$, we obtain the net force

$$k \delta z \equiv \alpha \gamma \delta z + \zeta \beta E_{\text{eq}}^{-\zeta-1} \gamma \delta z, \quad (\text{B2})$$

where $\alpha \gamma \delta z$ is the contribution due to F_E , i.e.,

$$\alpha\gamma\delta z \equiv ck\delta z. \quad (\text{B3})$$

Combining Eqs. (B2) and (B3) yields

$$c = \frac{1}{1 + \zeta}. \quad (\text{B4})$$

For $1 \leq \zeta \leq 2$, Eq. (B4) yields a minimum value, 0.3, for the parameter c . Thus, we estimate that $c \geq 0.3$, for $v_i/v_{Ti} \gg 2.5$.

- ¹C. K. Goertz, *Rev. Geophys.* **27**, 271, doi:10.1029/RG027i002p00271 (1989).
²G. Selwyn, J. McKillop, K. Haller, and J. Wu, *J. Vac. Sci. Technol. A* **8**, 1726 (1990).
³H. Thomas, G. Morfill, V. Demmel, J. Goree, B. Feuerbacher, and D. Möhlmann, *Phys. Rev. Lett.* **73**, 652 (1994).
⁴J. H. Chu and L. I., *Phys. Rev. Lett.* **72**, 4009 (1994).
⁵G. J. Kalman, P. Hartmann, Z. Donkó, and M. Rosenberg, *Phys. Rev. Lett.* **92**, 065001 (2004).
⁶A. Melzer, A. Homann, and A. Piel, *Phys. Rev. E* **53**, 2757 (1996).
⁷S. Zhdanov, S. Nunomura, D. Samsonov, and G. Morfill, *Phys. Rev. E* **68**, 035401(R) (2003).
⁸V. E. Fortov, A. G. Khrapak, S. A. Khrapak, V. I. Molotkov, and O. F. Petrov, *Phys. Usp.* **47**, 447 (2004).
⁹V. E. Fortov, A. V. Ivlev, S. A. Khrapak, A. G. Khrapak, and G. E. Morfill, *Phys. Rep.* **421**, 1 (2005); G. Morfill and A. Ivlev, *Rev. Mod. Phys.* **81**, 1353 (2009).
¹⁰Z. Donkó, P. Hartmann, and G. J. Kalman, *Phys. Rev. E* **69**, 065401(R) (2004).
¹¹P. Hartmann, G. J. Kalman, Z. Donkó, and K. Kutasi, *Phys. Rev. E* **72**, 026409 (2005).
¹²V. E. Fortov, O. S. Vaulina, and O. F. Petrov, *Plasma Phys. Controlled Fusion* **47**, B551 (2005).
¹³O. S. Vaulina, I. E. Drangevski, X. G. Adamovich, O. F. Petrov, and V. E. Fortov, *Phys. Rev. Lett.* **97**, 195001 (2006).
¹⁴B. Liu and J. Goree, *Phys. Rev. Lett.* **100**, 055003 (2008).
¹⁵O. Arp, D. Block, A. Piel, and A. Melzer, *Phys. Rev. Lett.* **93**, 165004 (2004).
¹⁶S. Nunomura, J. Goree, S. Hu, X. Wang, A. Bhattacharjee, and K. Avinash, *Phys. Rev. Lett.* **89**, 035001 (2002).
¹⁷S. Ratynskaia, K. Rypdal, C. Knapek, S. Khrapak, A. V. Milovanov, A. Ivlev, J. J. Rasmussen, and G. E. Morfill, *Phys. Rev. Lett.* **96**, 105010 (2006).
¹⁸S. Nunomura, D. Samsonov, S. Zhdanov, and G. Morfill, *Phys. Rev. Lett.* **96**, 015003 (2006).
¹⁹V. Nosenko, S. Zhdanov, A. V. Ivlev, G. Morfill, J. Goree, and A. Piel, *Phys. Rev. Lett.* **100**, 025003 (2008).
²⁰D. Samsonov, J. Goree, Z. W. Ma, A. Bhattacharjee, H. M. Thomas, and G. E. Morfill, *Phys. Rev. Lett.* **83**, 3649 (1999).
²¹B. Liu, J. Goree, V. E. Fortov, A. M. Lipaev, V. I. Molotkov, O. F. Petrov,

- G. E. Morfill, H. M. Thomas, H. Rothermel, and A. V. Ivlev, *Phys. Plasmas* **16**, 083703 (2009).
²²V. Nosenko and J. Goree, *Phys. Rev. Lett.* **93**, 155004 (2004).
²³B. Liu, K. Avinash, and J. Goree, *Phys. Rev. Lett.* **91**, 255003 (2003).
²⁴G. A. Hebner, M. E. Riley, D. S. Johnson, P. Ho, and R. J. Buss, *Phys. Rev. Lett.* **87**, 235001 (2001).
²⁵B. Liu, K. Avinash, and J. Goree, *Phys. Rev. E* **69**, 036410 (2004).
²⁶A. A. Samarian and B. W. James, *Phys. Lett. A* **287**, 125 (2001).
²⁷A. V. Ivlev, R. Sütterlin, V. Steinberg, M. Zuzic, and G. Morfill, *Phys. Rev. Lett.* **85**, 4060 (2000).
²⁸E. C. Whipple, *Rep. Prog. Phys.* **44**, 1197 (1981).
²⁹M. Wolter, A. Melzer, O. Arp, M. Klindworth, and A. Piel, *Phys. Plasmas* **14**, 123707 (2007).
³⁰H. M. Thomas, G. E. Morfill, V. E. Fortov, A. V. Ivlev, V. I. Molotkov, A. M. Lipaev, T. Hagl, H. Rothermel, S. A. Khrapak, R. K. Suetterlin, M. Rubin-Zuzic, O. F. Petrov, V. I. Tokarev, and S. K. Krikalev, *New J. Phys.* **10**, 033036 (2008).
³¹A. Melzer, T. Trottenberg, and A. Piel, *Phys. Lett. A* **191**, 301 (1994).
³²T. Trottenberg, A. Melzer, and A. Piel, *Plasma Sources Sci. Technol.* **4**, 450 (1995).
³³A. Homann, A. Melzer, and A. Piel, *Phys. Rev. E* **59**, R3835 (1999).
³⁴V. V. Yaroshenko, B. M. Annaratone, S. A. Khrapak, H. M. Thomas, G. E. Morfill, V. E. Fortov, A. M. Lipaev, V. I. Molotkov, O. F. Petrov, A. I. Ivanov, and M. V. Turin, *Phys. Rev. E* **69**, 066401 (2004).
³⁵M. Klindworth, O. Arp, and A. Piel, *J. Phys. D: Appl. Phys.* **39**, 1095 (2006).
³⁶V. A. Godyak and R. B. Piejak, *J. Appl. Phys.* **68**, 3157 (1990).
³⁷L. S. Frost, *Phys. Rev.* **105**, 354 (1957).
³⁸S. A. Khrapak, A. V. Ivlev, S. K. Zhdanov, and G. E. Morfill, *Phys. Plasmas* **12**, 042308 (2005).
³⁹H. Rothermel, T. Hagl, G. E. Morfill, M. H. Thoma, and H. M. Thomas, *Phys. Rev. Lett.* **89**, 175001 (2002).
⁴⁰Y. Feng, J. Goree, and B. Liu, *Rev. Sci. Instrum.* **78**, 053704 (2007).
⁴¹M. Schwabe, S. K. Zhdanov, H. M. Thomas, A. V. Ivlev, M. Rubin-Zuzic, G. E. Morfill, V. I. Molotkov, A. M. Lipaev, V. E. Fortov, and T. Reiter, *New J. Phys.* **10**, 033037 (2008).
⁴²S. A. Khrapak, S. V. Ratynskaia, A. V. Zobnin, A. D. Usachev, V. V. Yaroshenko, M. H. Thoma, M. Kretschmer, H. Höfner, G. E. Morfill, O. F. Petrov, and V. E. Fortov, *Phys. Rev. E* **72**, 016406 (2005).
⁴³T. E. Sheridan, *Phys. Rev. E* **72**, 026405 (2005).
⁴⁴S. Ratynskaia, S. Khrapak, A. Zobnin, M. H. Thoma, M. Kretschmer, A. Usachev, V. Yaroshenko, R. A. Quinn, G. E. Morfill, O. Petrov, and V. E. Fortov, *Phys. Rev. Lett.* **93**, 085001 (2004).
⁴⁵S. V. Annibaldi, A. V. Ivlev, U. Konopka, S. Ratynskaia, H. M. Thomas, G. E. Morfill, A. M. Lipaev, V. I. Molotkov, O. F. Petrov, and V. E. Fortov, *New J. Phys.* **9**, 327 (2007).
⁴⁶Y. Nakamura and O. Ishihara, *Phys. Plasmas* **16**, 043704 (2009).
⁴⁷C. Zafiu, A. Melzer, and A. Piel, *Phys. Rev. E* **63**, 066403 (2001).
⁴⁸J. Goree, G. E. Morfill, V. N. Tsytovich, and S. V. Vladimirov, *Phys. Rev. E* **59**, 7055 (1999).